ISSN: 2476-6909; Modares. Mech. Eng. 2027;27(04):297-313.

Modares Mechanical Engineering

DOI: 10.48311/mme.2026.122197.83061
journal homepage: mme.modares.ac.ir

Constraint-Controlled Optimization and Exergy Assessment of a Simple R1233zd(E) ORC For High-Temperature Exhaust Heat Recovery

Negin Sadat Hoseini Navid*, Reza Taghavi Zenouz

Department of Mechanical Engineering, Iran University of Science and Technology, Tehran, Iran

ARTICLE INFO

Article Type
Original Research

Article History
Received: June 30, 2026
Revised: September 26, 2026
Accepted: November 01, 2026
ePublished: November 13, 2026

ABSTRACT

High-temperature exhaust streams contain substantial recoverable energy, but simple organic Rankine cycle (ORC) performance is often governed by interacting thermal and fluid-property constraints. This study develops a physically constrained optimization, exergy assessment, and sensitivity framework for a simple subcritical ORC using low-global-warming-potential R1233zd(E). A fixed-composition natural-gas-turbine exhaust enters at 543 °C and 80.4 kg s^{-1}, with temperature-dependent properties evaluated using NASA7 ideal-gas correlations. The counter-flow heat-recovery vapor generator includes a 15 K pinch constraint, a 120 °C minimum stack temperature, and cooling-water approach limits. Decision variables are evaporation-pressure ratio, condensation temperature, and superheating degree; working-fluid properties are calculated with CoolProp 7.2.0. An independent numerical rerun reproduces the same constraint-controlled boundary design within numerical tolerance. The retained design delivers 6119.49 kW net power and 16.388% thermal efficiency at an evaporation-pressure ratio of 0.849996, condensation temperature of 38.000 °C, and 4.580 K superheating. The stack-temperature, condenser-approach, and critical-temperature safety constraints are active, while the actual minimum HRVG temperature difference is 80.18 K, confirming that the pinch constraint is inactive. The hot-gas physical-exergy decrease is about 18.22 MW, with a net physical-exergy recovery ratio of 33.58%. Exergy analysis identifies the HRVG as the main source of irreversibility. Overall, the results show that source–working-fluid temperature mismatch limits the suitability of a simple subcritical R1233zd(E) cycle for high-temperature exhaust recovery.

Keywords: Organic Rankine Cycle; R1233zd(E); Waste-Heat Recovery; Constrained Optimization; Exergy Analysis

How to cite this article
Hoseini Navid N S and Taghavi Zenouz R, Constraint-Controlled Optimization and Exergy Assessment of a Simple R1233zd(E) ORC For High-Temperature Exhaust Heat Recovery. Modares Mechanical Engineering; 2027;27(04):297-313.

*Corresponding author's email: n_hoseininavid@mecheng.iust.ac.ir
*Corresponding ORCID ID: 0009-0000-8841-8820

Copyright© 2027, TMU Press. This open-access article is published under the terms of the Creative Commons Attribution-NonCommercial 4.0 International License which permits Share (copy and redistribute the material in any medium or format) and Adapt (remix, transform, and build upon the material) under the Attribution-NonCommercial terms.

شاپا: ۶۹۰۹-۲۴۷۶؛ مهندسی مکانیک مدرس. ۳۱۳-۲۹۷:(۰۴)۲۷؛۱۴۰۶

مهندسی مکانیک مدرس

DOI: 10.48311/mme.2026.122197.83061

صفحه اصلی مجله: mme.modares.ac.ir

بهینه‌سازی کنترل‌شده با قیود و ارزیابی اگزرژی یک سیکل ساده رانکین آلی مبتنی بر سیال R1233zd(E) برای بازیابی حرارت گازهای خروجی دمابالا

نگین سادات حسینی نوید*، رضا تقوی زنوز

گروه مهندسی مکانیک، دانشگاه علم و صنعت ایران، تهران، ایران

اطلاعات مقاله

نوع مقاله
مقاله پژوهشی

تاریخچه مقاله
دریافت: ۱۴۰۵/۰۴/۰۹
بازنگری: ۱۴۰۵/۰۷/۰۴
پذیرش: ۱۴۰۵/۰۸/۱۰
ارائه آنلاین: ۱۴۰۵/۰۸/۲۲

چکیده

جریان‌های گاز خروجی دمای بالا ظرفیت قابل‌توجهی برای بازیابی انرژی دارند، اما عملکرد سیکل رانکین آلی (ORC) اغلب تحت اثر قیود حرارتی و خواص سیال قرار می‌گیرد. در این پژوهش، چارچوبی برای بهینه‌سازی مقید، ارزیابی اگزرژی و تحلیل حساسیت یک ORC زیربحرانی با سیال کم‌پتانسیل گرمایش جهانی R1233zd(E) توسعه یافته است. منبع حرارتی، گاز خروجی توربین گاز طبیعی با ترکیب ثابت، دمای ۵۴۳ درجه سلسیوس و دبی جرمی ۸۰/۴ کیلوگرم بر ثانیه است و خواص وابسته به دمای آن با روابط NASA7 محاسبه می‌شود. مولد بخار بازیاب حرارت جریان مخالف با قید پینچ ۱۵ کلوین، حداقل دمای دودکش ۱۲۰ درجه سلسیوس و محدودیت اختلاف دمای آب خنک‌کن مدل‌سازی شده است. متغیرهای تصمیم، نسبت فشار تبخیر، دمای چگالش و فوق‌گرمایش هستند و خواص سیال عامل با CoolProp 7.2.0 محاسبه می‌شوند. اجرای مستقل مجدد بهینه‌سازی، همان نقطه طراحی مرزی کنترل‌شده توسط قیود را در تلرانس عددی بازتولید کرد. این نقطه در نسبت فشار تبخیر ۰/۸۴۹۹۹۶، دمای چگالش ۳۸/۰۰۰ درجه سلسیوس و فوق‌گرمایش ۴/۵۸۰ کلوین، توان خالص ۶۱۱۹/۴۹ کیلووات و بازده حرارتی ۱۶/۳۸۸ درصد دارد. قیود دمای دودکش، اختلاف دمای کندانسور و حاشیه ایمنی دمای بحرانی فعال‌اند، اما حداقل اختلاف دمای واقعی HRVG برابر ۸۰/۱۸ کلوین است و غیرفعال بودن قید پینچ را نشان می‌دهد. کاهش اگزرژی فیزیکی گاز داغ حدود ۱۸/۲۲ مگاوات و نسبت بازیابی اگزرژی فیزیکی ۳۳/۵۸ درصد است. تحلیل اجزا، HRVG را منبع غالب برگشت‌ناپذیری نشان می‌دهد. نتایج نشان می‌دهند عدم تطابق دمایی منبع و سیال عامل، عملکرد ORC زیربحرانی R1233zd(E) را در بازیابی حرارت دمای بالا محدود می‌کند.

کلیدواژه‌ها: سیکل رانکین آلی؛ سیال R1233zd(E) ؛ بازیابی حرارت اتلافی؛ بهینه‌سازی مقید؛ تحلیل اگزرژی

نحوه ارجاع به این مقاله

حسینی نوید نگین سادات، تقوی زنوز رضا، «بهینه‌سازی کنترل‌شده با قیود و ارزیابی اگزرژی یک سیکل ساده رانکین آلی مبتنی بر سیال R1233zd(E) برای بازیابی حرارت گازهای خروجی دمابالا»، مهندسی مکانیک مدرس. ۳۱۳-۲۹۷:(۰۴)۲۷؛۱۴۰۶.

*پست الکترونیکی نویسنده عهده‌دار مکاتبات: n_hoseininavid@mecheng.iust.ac.ir

*شناسه ارکید نویسنده عهده‌دار مکاتبات: ۰۰۰۹-۰۰۰۰-۸۸۴۱-۸۸۲۰

Copyright© 2027, TMU Press. This open-access article is published under the terms of the Creative Commons Attribution-NonCommercial 4.0 International License which permits Share (copy and redistribute the material in any medium or format) and Adapt (remix, transform, and build upon the material) under the Attribution-NonCommercial terms.

Highlights

- A simple subcritical R1233zd(E) ORC is assessed as a constraint-dominated baseline for a 543 °C natural-gas-turbine exhaust source.
- Explicit constraint margins reveal a boundary solution governed by stack temperature, condenser approach and the fluid critical-temperature safety limit.
- The required HRVG pinch is 15 K, whereas the actual minimum temperature difference is 80.18 K, demonstrating that the heat-recovery process is not pinch-controlled.
- An independent NASA7-based optimization rerun reproduces the 6.119 MW constraint-controlled boundary solution within numerical tolerance.
- Component-level exergy analysis identifies the HRVG as the dominant irreversibility source, linking the main performance limitation to source–working-fluid temperature mismatch.

1- Introduction

Industrial exhaust streams from gas turbines, process heaters and high-temperature manufacturing equipment are important sources of recoverable energy [1]. Organic Rankine cycles (ORCs) are widely investigated for converting such waste heat into useful power [1, 2]. Organic fluids can be selected to match different heat-source levels and expander requirements [3, 4]. Recent comprehensive reviews and multi-criteria ORC studies also emphasize that working-fluid selection and design ranking should account for technical constraints and decision priorities rather than thermal efficiency alone [5, 6].

Working-fluid selection and operating-point optimization in ORCs are constrained by the heat-source temperature profile, condenser temperature, turbine outlet dryness, pressure ratio, heat-exchanger approach temperatures and fluid critical properties [3, 4]. For waste-heat recovery applications, cycle architecture and heat-exchanger arrangement also strongly affect the feasible operating window [7, 8]. For high-temperature exhaust recovery, these constraints are particularly important because a low-critical-temperature fluid can reach its allowable turbine-inlet temperature before the heat-source temperature profile is well matched in the HRVG [3, 8]. In that situation, a conventional pinch-based interpretation may be misleading if the actual pinch constraint is inactive [8].

R1233zd(E) has received attention as a low-GWP alternative to R245fa [9, 10]. Experimental studies have shown that R1233zd(E) can be used as a drop-in or replacement fluid in ORC systems, although its power output, efficiency and component behavior depend strongly on the heat source, heat exchangers and expander operating range [9–11]. Environmental and low-GWP screening studies have also identified R1233zd(E) as a relevant replacement candidate for R245fa-based ORC applications [12, 13]

1-1- Problem statement and contribution

Recent studies confirm that neither the optimization of a simple ORC nor the use of R1233zd(E) is novel by itself. Previous ORC process-optimization studies have explicitly treated interacting process and working-fluid constraints [14]. R1233zd(E) has already been investigated experimentally as a low-GWP replacement for R245fa under low- and moderate-temperature conditions, including studies of working-fluid mass flow rate, condensation conditions, expander operation, heat-exchanger behavior and material compatibility [9–12, 17]. More recently, R1233zd(E) has also been evaluated experimentally for engine waste-heat recovery [15] and investigated in thermoeconomic multi-objective studies of basic and regenerative ORC configurations [16]. Therefore, the present study does not claim novelty from simple-cycle optimization, differential-evolution optimization, or the generic concept of identifying active constraints. Instead, the unresolved question addressed here is how the interacting thermal and fluid-property constraints govern a simple subcritical R1233zd(E) cycle when it is deliberately coupled to a much hotter 543 °C exhaust stream.

Table 1 Positioning of the present study relative to representative constrained-ORC and R1233zd(E) studies

Study	Application / heat-source context	Working fluid / configuration	Main focus	Difference from the present study
Lampe et al. [14]	Geothermal ORC	Simultaneous working-fluid and process optimization	Integrated fluid/process optimization and analysis of active constraint sets	General ORC optimization framework; not R1233zd(E) and not a 543 °C exhaust-source mismatch
Eyerer et al. [9]	Low-temperature heat utilization	R1233zd(E) and R245fa; experimental ORC	Drop-in replacement, operating parameters, efficiency and power	Experimental replacement study; no high-temperature constraint diagnosis
Yang et al. [10]	Low-temperature ORC application	R1233zd(E) and R245fa	Experimental comparison and optimization guidance	Focused on replacement performance and expander/heat-exchanger behavior rather than high-temperature boundary constraints
Eyerer et al. [11]	Low-temperature heat utilization	R1224yd(Z), R1233zd(E) and R245fa	Experimental performance and replacement suitability	No 543 °C exhaust source and no simultaneous stack/critical-temperature constraint diagnosis
Zhang et al. [15]	Engine waste-heat recovery	R1233zd(E) and R123; experimental ORC	Performance comparison over multiple engine loads	Experimental engine-WHR comparison; does not quantify the present MW-scale high-temperature boundary optimum and HRVG exergy mismatch
Li et al. [16]	Low-temperature waste-heat recovery	Basic, regenerative and extraction-regenerative R1233zd(E) ORCs	Thermoeconomic multi-objective optimization	Focuses on low-temperature thermoeconomics and configuration selection rather than high-temperature active-constraint diagnosis
Present study	543 °C exhaust stream	Simple subcritical R1233zd(E) ORC	Constraint-margin diagnosis, counter-flow HRVG temperature matching and exergy destruction	Shows simultaneous stack, condenser and critical-temperature limitation, an inactive 15 K HRVG pinch, and quantifies the resulting HRVG exergy penalty

The selection of R1233zd(E) in the present study should not be interpreted as an a priori claim that an organic Rankine cycle is superior to a conventional water/steam Rankine cycle for a 543 °C heat source. Water/steam is a relevant candidate at this source-temperature level because it can accommodate substantially higher turbine-inlet temperatures than R1233zd(E). However, the preferred waste-heat-recovery cycle cannot be determined from source inlet temperature alone; it also depends on heat-source characteristics, temperature matching, operating conditions, system scale and cycle architecture [4, 7]. The purpose of using R1233zd(E) here is therefore diagnostic rather than comparative: the fluid provides a low-GWP, experimentally established ORC baseline for quantifying how a relatively low critical temperature constrains the utilization of a much hotter exhaust stream. The results are subsequently interpreted as a

limitation assessment of this specific simple ORC rather than as evidence of superiority over a steam Rankine cycle.

Accordingly, the contribution of the present study lies in the constraint-level diagnosis of the high-temperature source–R1233zd(E) interaction rather than in the optimization algorithm itself. This interpretation is further examined through a same-source literature benchmark with an independently optimized subcritical toluene ORC, which has a substantially higher critical temperature than R1233zd(E). For the identical exhaust-source conditions of 543 °C and 80.4 kg s^{-1}, the published toluene case reaches a considerably higher turbine-inlet temperature, providing independent support for the conclusion that the relatively low critical temperature of R1233zd(E) aggravates the source–working-fluid temperature mismatch. Because the two studies employ different heat-transfer and heat-rejection arrangements, this comparison is used as supporting thermodynamic evidence rather than as a controlled fluid-only performance ranking.

2- System description and modeling assumptions

The investigated system is a simple subcritical ORC driven by the exhaust of an industrial SGT-600-class natural-gas turbine. The adopted heat-source conditions are an exhaust-gas inlet temperature of 543 °C and a mass flow rate of 80.4 kg s^{-1}. Rather than representing the heat source as air with a constant effective heat capacity, the revised model treats the exhaust as a fixed-composition combustion-product mixture consisting of 75.4 mol.% N_2, 13.6 mol.% O_2, 3.4 mol.% CO_2, 6.6 mol.% H_2O and 1.0 mol.% Ar [18]. Temperature-dependent ideal-gas properties of the individual species are evaluated using NASA7 polynomial correlations, and the corresponding mixture enthalpy, entropy and heat capacity are calculated from the species properties [19]. The exhaust gas enters the counter-flow HRVG at 543 °C and is cooled to the imposed minimum stack temperature of 120 °C when the stack-temperature constraint is active.

The ORC consists of a pump, HRVG, turbine and condenser. State 1 is saturated liquid at the condenser outlet, state 2 is compressed liquid at the pump outlet, state 3 is saturated vapor at the evaporation pressure, state 4 is the superheated turbine inlet, state 5 is the turbine outlet and state 6 is the condenser inlet after a small pressure adjustment. The revised cycle model assumes steady-state operation and fixed pump and turbine isentropic efficiencies. Detailed geometry-dependent pressure and heat losses are not included in the reference optimization; their influence is quantified separately through the pressure-drop and heat-loss sensitivity analysis.

Thermophysical properties were evaluated using CoolProp 7.2.0 with the default HEOS backend through the Python interface in MATLAB. The same backend was used consistently throughout the calculations to maintain internal consistency between the optimized state points and the critical-property constraints. The critical temperature and critical pressure reported in Table 2 were taken from the same CoolProp 7.2.0 backend used during the optimization. This is important because the optimized turbine-inlet temperature lies very close to the imposed critical-temperature safety boundary; therefore, changing the property database or backend may slightly shift the numerical optimum. The present results should consequently be interpreted as property-backend-consistent cycle-level predictions rather than as database-independent component validation.

3- Methodology

3-1- Thermodynamic and exergy models

All thermodynamic properties of R1233zd(E) are evaluated using CoolProp 7.2.0 with the default HEOS backend through the Python interface in MATLAB [20]. The pump and turbine are modeled using fixed isentropic efficiencies following standard ORC cycle-level modeling practice [4]. The main first-law relations are written in numbered form to improve reproducibility and journal formatting.

$$w_p = h_2 - h_1 , \dot{W}_p = \dot{m}_{ORC} (h_2 - h_1) \quad (1)$$

$$w_t = h_4 - h_5 , \dot{W}_t = \dot{m}_{ORC} (h_4 - h_5) \quad (2)$$

$$\dot{W}_{net} = \dot{W}_t - \dot{W}_p \quad (3)$$

$$\dot{Q}_{in} = \dot{m}_{ORC} (h_4 - h_2) \quad (4)$$

$$\eta_{th} = \frac{\dot{W}_{net}}{\dot{Q}_{in}} \quad (5)$$

Table 2 Final data input used in the R1233zd(E) fixed-pinch counter-flow ORC optimization.

Parameter	Value	Unit
Working fluid	R1233zd(E)	-
HRVG flow arrangement	Counter-flow	-
Heat source type	SGT-600-derived natural-gas-turbine exhaust	-
Hot-gas inlet temperature	543	°C
Hot-gas mass flow rate	80.4	kg s^{-1}
Exhaust N2 mole fraction	75.4	mol.%
Exhaust O_2 mole fraction	13.6	mol.%
Exhaust CO_2 mole fraction	3.4	mol.%
Exhaust H_2O mole fraction	6.6	mol.%
Exhaust Ar mole fraction	1.0	mol.%
Hot-gas property model	Temperature-dependent NASA7 ideal-gas mixture	-
Mixture molecular weight	28.5588	kg $kmol^{-1}$
Mean cp, 120–543 °C	1.09799	kJ kg^{-1} K^{-1}
Minimum stack temperature	120	°C
Cooling-water inlet temperature	25	°C
Cooling-water nominal outlet temperature	30	°C
Minimum condenser approach	8	K
Fixed HRVG pinch point	15	K
Turbine isentropic efficiency	0.85	-
Pump isentropic efficiency	0.75	-
HRVG working-fluid pressure-drop ratio, reference case	0	-
Pressure-drop ratios examined in sensitivity analysis	0.01, 0.03, 0.05	
External HRVG heat-loss fraction examined	0, 0.01, 0.02	
Minimum turbine-outlet dryness indicator	0.88	-
Critical-temperature safety margin	5	K
Critical temperature	439.6008	K
Critical pressure	36.2369	bar
Number of HRVG/condenser discretization points	140	-
Property database/backend	CoolProp 7.2.0, default HEOS backend through Python interface in MATLAB	-
Critical-property source	Same CoolProp 7.2.0 backend used in the optimization	-

To quantify the influence of working-fluid pressure losses without introducing unsupported geometry-dependent correlations, a fixed-design pressure-drop sensitivity was performed around the revised operating point.

The optimized decision variables were held unchanged during this analysis. A fractional pressure loss δ_{HRVG} was imposed between the pump-discharge/evaporation-pressure level and the turbine inlet, while the existing low-side pressure adjustment was generalized through δ_{low} . The corresponding turbine pressure levels are represented by

$$P_{t,in} = (1- \delta_{HRVG})P_{evap} \quad (6)$$

$$P_{t,out}= \frac{P_{cond}}{1-\delta_{low}} \quad (7)$$

$$\Pi_t= \frac{P_{t,in}}{P_{t,out}} \quad (8)$$

For each prescribed pressure-loss case, the turbine expansion calculation is repeated while the optimized values of r_{evap}, ΔT_{cond} and ΔT_{sh} are kept fixed. Hence, the analysis represents a pressure-loss sensitivity of the optimized design and not a separate re-optimization. Pressure-drop ratios of 1%, 3% and 5% were selected to span mild to deliberately conservative screening conditions.

External thermal loss from the HRVG was examined separately using

$$\dot{Q}_{ORC}=(1- f_Q)\, \dot{Q}_{HRVG} \quad (9)$$

where f_Q denotes the fractional external HRVG heat loss. Values of 0, 0.01 and 0.02 were examined. This simple formulation is intended only to quantify the first-order sensitivity to imperfect insulation; detailed heat-exchanger design would require geometry- and ambient-dependent heat-loss correlations.

The HRVG is modeled as a counter-flow heat exchanger, consistent with common ORC waste-heat-recovery modeling practice [4, 8]. Because the exhaust-gas heat capacity varies with temperature, the hot-stream temperature profile is evaluated from the temperature-dependent mixture enthalpy rather than from a constant-cpc_p linear relation. The cumulative heat-transfer coordinate Q is measured from the cold end of the HRVG. For the fixed exhaust composition, the local hot-stream state satisfies

$$\dot{Q}= \dot{m}_h[h_h(T_h)- h_h\,(T_{h,out})] \quad (10)$$

and the corresponding local hot-stream temperature is obtained from

$$T_h\,(\dot{Q})= h_h^{-1}[h_h\,(T_{h,out})+ \frac{\dot{Q}}{\dot{m}_h}] \quad (11)$$

Here, $h_{h(T)}$ is the temperature-dependent specific enthalpy of the combustion-product mixture calculated from the NASA7 species correlations. The local counter-flow temperature difference is then

$$\Delta T_{HRVG}\,(\dot{Q})= T_h\,(\dot{Q})- T_{wf}\,(\dot{Q}) \quad (12)$$

and the HRVG feasibility constraint is

$$\min_{0\le \dot{Q}\le \dot{Q}} [\Delta T_{HRVG}(\dot{Q})] \ge \Delta T_{pinch,fixed} \quad (13)$$

The preliminary four-variable trial showed that the HRVG pinch did not control the optimum. Therefore, the final decision vector is deliberately reduced to three variables, while the HRVG pinch is fixed at 15 K. This avoids assigning physical significance to a numerically arbitrary inactive design variable:

$$x = [r_{evap},\, T_{cond},\, \Delta T_{sh}]^T,\, \Delta T_{pinch,fixed}= 15\ \text{K} \quad (14)$$

The feasibility constraints imposed on each candidate solution are:

$$T_{hot,out} \ge T_{stack,min} \quad (15)$$

$$T_{cond} - T_{cw,out} \ge \Delta T_{app,min} \quad (16)$$

$$T_{turbine,in} \le T_{crit} - \Delta T_{crit,margin} \quad (17)$$

$$q_{turbine,out} \ge q_{min} \quad (18)$$

The specific physical exergy of a stream is evaluated relative to an environmental reference temperature $T_0 = 298.15$ K using the standard physical-exergy formulation for steady-flow systems [4]. For the working fluid, only exergy differences are required, so the CoolProp reference-state offset cancels:

$$e = (h - h_0) - T_0\,(s - s_0) \quad (19)$$

For the fixed-composition exhaust mixture cooling at approximately constant pressure, the physical-exergy decrease is evaluated directly from the temperature-dependent mixture enthalpy and entropy rather than from a constant-c_p approximation:

$$\Delta \dot{E}^{ph}_{x,h} = \dot{m}_h\{[h_h(T_{in}) - h_h(T_{out})] - T_0[sh(T_{in,ph} - s_h(T_{out,ph})] \quad (20)$$

The exhaust composition is unchanged across the HRVG and the gas-side pressure variation is neglected at this cycle-model level; consequently, constant composition-dependent reference terms cancel in the inlet-to-outlet physical-exergy difference. The mixture enthalpy and entropy are evaluated using the same temperature-dependent NASA7 property model employed for the HRVG temperature profile. All temperatures entering the exergy calculation are expressed on an absolute Kelvin scale. Chemical exergy is not included because the present metric considers only the physical exergy decrease associated with cooling of the unchanged exhaust mixture.

Component exergy destruction is obtained from steady-state exergy balances [4]. To quantify the fraction of the exhaust physical-exergy decrease converted into net ORC power, the following net physical-exergy recovery ratio is defined:

$$\psi_{rec}= \frac{\dot{W}_{net}}{\Delta \dot{E}^{ph}_{x,h}} \quad (21)$$

where $\dot{W}_{net}$ is the turbine power output minus the ORC working-fluid pump power, and $\Delta \dot{E}^{ph}_{x,h}$ is the physical-exergy decrease of the fixed-composition exhaust stream between the HRVG inlet and outlet. This ratio is used as a cycle-level recovery metric and is not intended as a complete plant exergetic efficiency [22]. It excludes balance-of-plant auxiliary power, external cooling-water pumping and chemical exergy of the exhaust, and it does not account for the physical exergy remaining in the discharged stack gas.

3-2- Numerical workflow and optimization strategy

The numerical workflow consisted of feasibility screening, differential-evolution optimization, Morris-type constrained screening and local one-at-a-time (OAT) sensitivity analysis. The final decision vector was x = [r_{evap}, T_{cond}, ΔT_{sh}], while the HRVG pinch was fixed at 15 K and retained only as a feasibility constraint. The search bounds were r_{evap} = 0.30–0.85, T_{cond} = 25–60 °C and ΔT_{sh} = 0–30 K. The feasibility scan used 3000 uniformly sampled random design points over this three-variable domain with a fixed random seed of 42. The HRVG and condenser temperature profiles were discretized using 140 points, as reported in Table 2.

The net-power maximization was implemented as the minimization of $\dot{W}_{net}$ using a custom differential-evolution (DE) solver written in MATLAB, following the classical DE framework of Storn and Price [21]. The DE control parameters were fixed a priori and were not treated as optimization variables or tuned against the final optimum. The mutation factor (F=0.70) was selected within the range commonly used in classical DE [21], while a relatively high crossover probability of (CR=0.90) was adopted because the three decision variables are thermodynamically coupled through the feasibility constraints. The population size was fixed at 50 individuals, the initial population was sampled uniformly over the complete variable bounds, and a fixed computational budget of 120 generations was used. The random seed was set to 123 solely to make the reported search reproducible.

Constraint handling was implemented through a penalty objective. A candidate was considered feasible only when the stack-temperature, condenser-approach, turbine-outlet dryness, critical-temperature, and HRVG-pinch margins were all greater than or equal to -10^{-6} and the net power was positive. Feasible candidates were assigned the objective value $\dot{W}_{net}$. Infeasible candidates were assigned a large penalty of $10^{13} + 10^{12}\sum_i v_i^2 + 10^{10}N_v$, where v_i are the normalized

positive constraint violations and N_v is the number of violated constraints. The normalization scales used for the stack-temperature, condenser-approach, dryness, critical-temperature, and HRVG-pinch margins were 10 K, 5 K, 0.05, 5 K, and 5 K, respectively. Candidates that produced CoolProp or numerical failures were assigned a penalty of 10^{15}.

The Morris-type constrained screening followed the elementary-effects philosophy of Morris [22], but it was implemented as a constrained continuous screening rather than as a discrete grid-level Morris design. Sixty random normalized base points were generated using a fixed seed of 777, and a normalized perturbation size of 0.20 was applied to one variable at a time. Elementary effects were retained only when both the base and perturbed points were feasible. The local OAT sensitivity used perturbations equal to 10% of each variable range, corresponding to 0.055 for r_{evap}, 3.5 °C for T_{cond}, and 3.0 K for ΔT_{sh}.

Following replacement of the exhaust representation by the fixed-composition NASA7 model, an independent numerical cross-check was reconstructed from the reported governing equations, the CoolProp 7.2.0/HEOS R1233zd(E) property representation, the stated decision-variable bounds, and the principal thermodynamic constraint definitions. The cross-check included a 3000-point feasibility scan, a differential-evolution rerun using the stated DE control parameters, Morris-type screening, and local OAT analysis. It was used to determine whether the previously identified constraint-controlled boundary solution and sensitivity structure remained reproducible under the revised temperature-dependent source-property formulation. Because this cross-check was implemented independently from the original MATLAB optimization workflow, the resulting convergence trajectory is interpreted as numerical reproducibility evidence rather than as a bitwise reproduction of the original solver execution.

3-3- Preliminary economic assessment

A screening-level economic assessment was added to evaluate whether the revised thermodynamic performance corresponds to a potentially meaningful waste-heat-recovery investment. Because detailed equipment sizing, vendor quotations and site-specific installation costs are outside the scope of the present cycle-level model, the economic analysis is intentionally formulated as a preliminary feasibility assessment rather than a bankable project estimate. The waste-heat input is assigned zero fuel cost because it is assumed to be otherwise rejected to the environment.

The installed-capital-cost range was selected from industrial ORC waste-heat-recovery data. The TASIO project reports total CAPEX of approximately 2.2–3.3 M€ MW−1 for the indirect-exchange configuration (ORC plus heat-recovery system), while operating expenditure for direct exchange is reported as approximately 1–1.5% of CAPEX [23]. Accordingly, 2.75 M€ MW^{-1} and 1.25% yr^{-1} are adopted as the baseline specific investment cost and O&M fraction, respectively, while the reported ranges are retained for sensitivity analysis. These values are used only as literature-based screening parameters and do not constitute vendor quotations for the present plant.

A project lifetime of 20 years, 8000 annual operating hours, and a real discount rate of 8% are adopted as screening assumptions in the present study. The annual electricity generation is calculated as:

$$E_{ann} = \dot{W}_{net} t_{op} \tag{22}$$

Where E_{ann} is the annual electricity generation, $\dot{W}_{net}$ is the net cycle power output, and t_{op} is the annual operating time.

The capital recovery factor is calculated as :

$$CRF = \frac{i(1+i)^N}{(1+i)^N - 1} \tag{23}$$

where i is the real annual discount rate and N is the project lifetime in years.

Table 3 Assumptions adopted for the preliminary economic screening.

Parameter	Baseline	Sensitivity range
Net cycle power	6.11949 MW	fixed at revised design
Annual operating time	8000 h/y	–
Project lifetime	20 y	–
Real discount rate	8%	–
Specific installed capital cost	2.75 M€/MW	2.20–3.30 M€/MW
Annual O&M cost	1.25% of CAPEX	1.0–1.5%
Waste-heat fuel cost	0	–
Electricity value	0.10 €/kWh	0.06–0.12 €/kWh

The screening-level levelized cost of electricity is evaluated as:

$$LCOE = \frac{C_0 CRF + C_{O\&M}}{E_{ann}} \tag{24}$$

Where C_0 is the installed capital cost. For the cost-benefit assessment, the simple payback period and net present value are calculated as:

$$SPB = \frac{C_0}{p_e E_{ann} - C_{O\&M}} \tag{25}$$

And

$$NPV = -C_0 + \sum_{y=1}^{N} \frac{p_e E_{ann} - C_{O\&M}}{(1+i)^y} \tag{26}$$

where p_e denotes the avoided or credited electricity value and y represents the project year. Because the electricity value is strongly site- and market-dependent, no single local tariff is assumed; instead, values ranging from 0.06 to 0.12 € kWh^{-1} are examined parametrically.

Taxes, financing structure, electricity-price escalation, carbon-credit revenue, equipment replacement costs, and external cooling-system auxiliary power are excluded from the present screening analysis. Consequently, the resulting economic indicators should be interpreted as preliminary screening estimates rather than as complete plant-level financial metrics.

4- Model verification, literature benchmark, and uncertainty assessment

4-1- Verification and benchmark strategy

A directly matching published experimental or numerical dataset reproducing the complete 543 °C, 80.4 kg s^{-1} R1233zd(E) configuration and its constraints was not identified; therefore, one-to-one validation of the optimized high-temperature case is not claimed. Instead, the verification strategy is formulated as a multi-level procedure. First, internal first-law balance closure is checked at the optimized operating point. Second, the thermodynamic calculation framework is subjected to a direct R1233zd(E) numerical benchmark by reconstructing the non-recuperative ORC case reported by Braimakis and Karellas [24] under the same published boundary conditions. Third, the previously retained R245fa experimental reconstruction is used as an independent model-consistency check. Fourth, the broader applicability and reported performance trends of R1233zd(E) are assessed against published experimental and numerical studies [9–11,13,14]. This hierarchy distinguishes direct numerical reproduction, cross-fluid framework verification, literature benchmarking and direct experimental validation of the present high-temperature application.

In addition to the low-temperature fluid-specific reconstruction described below, a high-temperature same-fluid benchmark was identified in the work of Mariani et al. [29]. That study investigated a single-pressure R1233zd(E) ORC driven by experimentally characterized exhaust from a compression-ignition engine. The 75% engine-load condition is particularly relevant to the present work because the measured exhaust-gas temperature was approximately 532 °C, only 11 °C below the 543 °C source temperature adopted here. The published R1233zd(E) cycle operated at a maximum pressure of 3.0 MPa, a condensation pressure of 0.3 MPa, a turbine-inlet temperature of 433 K, and turbine and pump isentropic efficiencies of 0.80 and 0.75, respectively. For the single-pressure configuration at

Table 4 Validation hierarchy adopted for the present ORC model.

Validation level	What is checked	Quantitative result in the present work	Interpretation
First-law balance closure	Consistency between turbine work, pump work, HRVG heat input and condenser heat rejection	W_t=6590.29 kW, W_p=470.80, W_{net}=6119.49; $Q_{in}-Q_{out}$≈37341.86−31222.37=6119.49kW	Strong internal energy-balance verification
Direct R1233zd(E) numerical benchmark	Reproduction of an independently published non-recuperative R1233zd(E) ORC using the reported boundary conditions [24]	Published/reconstructed net electric power: 7.680/7.679 kWe (−0.018%); working-fluid flow: 0.450/0.4495 kg s^{-1} (−0.103%); expander hydraulic power: 8.970/8.972 kW (+0.018%)	Strong direct cross-model verification of the R1233zd(E) thermodynamic calculation framework; not experimental validation of the present 543 °C case
High-temperature same-fluid near-source benchmark	Single-pressure R1233zd(E) ORC under a measured high-temperature engine-exhaust condition close to the present source temperature [29]	$T_{exh,in}$=532∘C; P_{high}=30.0; $T_{turb,in}$=159.85∘C; $\dot{m}_{wf}$=2.20 kg s^{-1}; $\dot{Q}_{in}$=511kW; η_{th}=16.0%; corresponding $\dot{W}_{net}$=81.76 kW	High-temperature same-fluid quantitative benchmark with source temperature only 11°C below the present 543°C case; not exact MW-scale experimental validation
R245fa-based model-consistency check	Ability of the same ORC modeling framework to reproduce an experimentally reported small-scale case [25]	Nominal reconstructed case: 5.214 kW versus 5.405 kW, error = -3.53%; best-agreement case: 5.497 kW, error = +1.70% [25]	Indirect check of the cycle calculation framework and turbine-efficiency range
R1233zd(E) literature benchmark	Fluid applicability, replacement behavior and reported trends relative to R245fa	Published studies report R1233zd(E) as an ORC-capable low-GWP replacement; reported efficiency advantages range from about 2% to 6.92% in selected drop-in studies [9, 10, 17]	Fluid-level benchmark, not direct validation of the 543 °C MW-scale case
Exact 543 °C, MW-scale R1233zd(E) case	Direct experimental reproduction of the same heat-source temperature, scale and constraints	No directly matching open dataset identified	Remaining limitation; future direct validation is required before equipment-level design conclusions

75% engine load, the reported working-fluid mass flow rate and recovered heat were 2.20 kg s^{-1} and 511 kW, respectively, while the reported thermal efficiency was approximately 16.0%. These conditions provide a substantially closer high-temperature benchmark for the present application than the available low-temperature R1233zd(E) datasets, although differences in cycle scale, condenser condition and component efficiencies prevent this comparison from being interpreted as direct experimental validation of the complete present 543 °C MW-scale system.

4-2- Direct R1233zd(E) numerical benchmark

To provide a fluid-specific quantitative verification of the present thermodynamic calculation framework, an independent R1233zd(E) ORC case reported by Braimakis and Karellas [24] was reconstructed. Their non-recuperative CHP-mode ORC provides a suitable benchmark because the working fluid, principal state conditions, component efficiencies, heat input and several independent cycle outputs are explicitly reported. The published boundary conditions were imposed directly rather than adjusted to improve agreement.

The benchmark employs R1233zd(E) with an ORC heat input of 100 kW, an evaporation pressure of 17.35 bar, a turbine-inlet temperature of 130 °C, a condensation pressure of 3.62 bar, 5 K superheating, 5 K subcooling, and isentropic expander and pump efficiencies of 0.65. The published generator and pump-motor efficiencies of 0.96 and 0.85, respectively, were also retained. Thermophysical properties in the present reconstruction were evaluated using the same CoolProp 7.2.0 HEOS framework adopted throughout this manuscript, whereas the reference study employed REFPROP Table 5 compares the reconstructed outputs with the independently published values. The reconstructed net electric output is 7.6786 kWe compared with the reported 7.680 kWe, corresponding to a relative deviation of −0.018%. The working-fluid mass flow rate differs by −0.103%, while the expander hydraulic power differs by only +0.018%. The largest deviation among the reported power quantities is approximately 0.51% for the pump hydraulic power. The total reconstructed condenser-plus-subcooler heat rejection is 91.822 kW compared with the published total of 91.83 kW.

The close agreement across mass flow rate, expander work, pump work, net electrical output and heat rejection provides a direct quantitative cross-model benchmark for the R1233zd(E) cycle calculations. The remaining small deviations are consistent with differences in property libraries and rounding of the published boundary conditions and results. This comparison verifies the thermodynamic calculation framework under an independent R1233zd(E) operating case; however, it should not be interpreted as direct experimental validation of the present 543 °C, MW-scale exhaust application.

4-3- R245fa-based model-consistency check

The retained R245fa comparison is used strictly as a model-consistency check, not as direct validation of the present R1233zd(E) high-temperature exhaust case. For the nominal reconstructed case of Li et al. [25], P_{evap} = 15.00 bar, pressure ratio = 7.3 and pinch = 10.0 K give a model turbine power of 5.214 kW compared with the

Table 5 Direct numerical benchmark of the R1233zd(E) ORC calculation framework against the published non-recuperative case of Braimakis and Karellas [24]

Quantity	Published value	Present reconstruction	Deviation (%)
ORC heat input (kW)	100	100	imposed
Evaporation pressure (bar)	17.35	17.35	imposed
Turbine-inlet temperature (°C)	130	130	imposed
Condensation pressure (bar)	3.62	3.62	imposed
Superheating (K)	5	5	imposed
Subcooling (K)	5	5	imposed
Expander isentropic efficiency	0.65	0.65	imposed
Pump isentropic efficiency	0.65	0.65	imposed
Working-fluid mass flow rate (kg s^{-1})	0.450	0.44954	−0.103
Expander hydraulic power (kW)	8.970	8.97163	+0.018
Expander-generator output (kWe)	8.610	8.61276	+0.032
Pump hydraulic power (kW)	0.790	0.79404	+0.512
Pump electrical input (kWe)	0.930	0.93417	+0.448
Net electric output (kWe)	7.680	7.67859	−0.018
Condenser + sub-cooler heat rejection (kW)	91.830	91.8224	−0.008
Electric efficiency (–)	0.077	0.076786	−0.278

Table 6 High-temperature same-fluid comparison between the single-pressure R1233zd(E) case of Mariani et al. [29] and the present 543 °C simple ORC.

Quantity	Mariani et al. [29], 75% load	Present 543 °C case	Difference / relevance
Working fluid	R1233zd(E)	R1233zd(E)	Identical
Configuration	Single-pressure ORC	Simple subcritical ORC	Closely matched
Exhaust inlet temperature (°C)	532	543	11 °C (2.07%)
Maximum / evaporation pressure (bar)	30.0	30.8012	2.67%
Turbine-inlet temperature (°C)	159.85	161.4508	1.60 °C (1.00%)
Condensation pressure (bar)	3.0	2.0212	Different
Condensation temperature (°C)	50.85	38.00	Different
Turbine isentropic efficiency	0.80	0.85	Different
Pump isentropic efficiency	0.75	0.75	Identical
Working-fluid mass flow rate (kg s^{-1})	2.20	151.4176	Scale-dependent
Heat input (kW)	511	37341.86	Scale-dependent
Thermal efficiency (%)	16.0	16.3877	+0.388 percentage point
Net power (kW)	81.76*	6119.491	Scale-dependent
Specific heat input (kJ kg^{-1})	232.273*	246.615	–
Specific net work (kJ kg^{-1})	37.164*	40.415	–

❋Calculated from the heat-input, working-fluid mass-flow-rate, and thermal-efficiency data reported by Mariani et al. [29]. These derived quantities are included only to facilitate normalized comparison and were not reported explicitly in the original study.

reported experimental value of 5.405 kW. The relative deviation, calculated as (model - experiment)/experiment, is -3.53%, and the implied turbine isentropic efficiency is 0.829. A best-agreement reconstructed case with P_{evap} = 15.50 bar and pinch = 7.5 K gives 5.497 kW, corresponding to a relative deviation of +1.70% and an implied turbine efficiency of 0.787. These two comparisons show that the cycle model reproduces the correct order of magnitude and a physically reasonable turbine-efficiency range for an experimentally documented ORC system [25].

The R245fa benchmark therefore supports the numerical consistency of the ORC calculation framework, including pump/turbine work calculation, heat-addition balance and the use of isentropic-efficiency assumptions. It should not be interpreted as fluid-specific validation for R1233zd(E), because R1233zd(E) has different saturation properties, pressure levels, expander behavior and heat-transfer characteristics.

4-4- High-temperature same-fluid benchmark

Previous experimental and numerical studies have established R1233zd(E) as a technically viable low-GWP working fluid for ORC applications and as a potential replacement for R245fa under a range of low- and moderate-temperature operating conditions [9–13, 17]. However, these studies generally involve substantially lower source temperatures and smaller system scales than the present 543 °C application. Therefore, they are used here primarily to support fluid applicability rather than as direct quantitative validation of the present high-temperature case.

To extend the verification basis toward a source-temperature range closer to that considered in the present study, a quantitative comparison was performed against the R1233zd(E) ORC investigated by Mariani et al. [29]. Their study considered a single-pressure ORC driven by experimentally characterized compression-ignition-engine exhaust and therefore provides an independent same-fluid benchmark under high-temperature waste-heat-recovery conditions. At the selected 75% engine-load condition, the exhaust inlet temperature was approximately 532 °C, only 11 °C below the 543 °C source temperature considered here.

As summarized in Table 6, the reference R1233zd(E) cycle operated at a maximum pressure of 30.0 bar, compared with an evaporation pressure of 30.8012 bar in the present design. The corresponding turbine-inlet temperatures are 159.85 °C and 161.4508 °C, respectively. Thus, both the high-side pressure and the turbine-inlet temperature are closely matched. The pump isentropic efficiency is also identical at 0.75, whereas the reference turbine efficiency is 0.80 compared with 0.85 in the present model. The principal differences arise from the condensation condition and the substantially different system scale.

For the 75% engine-load condition, Mariani et al. [29] report a heat input of 511 kW and an R1233zd(E) mass flow rate of 2.20 kg s^{-1} for the single-pressure cycle, together with a thermal efficiency of approximately 16.0%. These values correspond to a calculated net cycle power of approximately 81.76 kW, a specific heat input of 232.273 kJ kg^{-1}, and a specific net work of 37.164 kJ kg^{-1}. For comparison, the present cycle gives a thermal efficiency of 16.3877%, a specific heat input of 246.615 kJ kg^{-1}, and a specific net work of 40.415 kJ kg^{-1}.

The close agreement in working fluid, cycle architecture, source-temperature level, high-side pressure, and turbine-inlet temperature provides a substantially more representative high-temperature benchmark than the low-temperature R1233zd(E) cases typically available in the literature. Nevertheless, the differences in system scale, condensation condition, expander efficiency, and heat-source characteristics prevent the comparison from being interpreted as an exact one-to-one experimental validation of the present 543 °C MW-scale ORC. It is therefore classified as a high-temperature same-fluid quantitative benchmark rather than as direct experimental validation.

Together with the independent R1233zd(E) numerical reconstruction in Section 4-2 and the experimental R245fa model-consistency check, this comparison broadens the verification basis of the present model from low-temperature cycle calculations to a high-temperature R1233zd(E) waste-heat-recovery application. Direct experimental validation of the complete present 543 °C MW-scale configuration remains unavailable and is retained as a limitation of the study.

4-5- First-law balance closure and exergy-balance residual

At the revised baseline operating point, the first-law balance closes within the reporting precision of the manuscript. The turbine power is 6590.293 kW and the pump power is 470.801 kW, giving a net power of 6119.491 kW. The HRVG heat input is 37341.86 kW and the condenser heat rejection is 31222.373 kW; their difference is approximately 6119.49 kW, in agreement with the reported net power within rounding precision. This confirms the internal energy-balance consistency of the revised cycle evaluation.

For the revised exergy assessment, the listed HRVG, turbine, pump and condenser exergy destructions sum to approximately 11816.94 kW. The difference between the hot-gas physical-exergy decrease, the net power and the listed component exergy destructions is $18222.88-6119.491-11816.94\approx286.45$ kW, corresponding to approximately 1.57% of the hot-gas physical-exergy decrease. This residual is sufficiently small for the stated component-level interpretation and is attributed to the simplified treatment of auxiliary streams, pressure-adjustment states and numerical rounding. The HRVG exergy destruction is approximately 9491.32 kW, corresponding to about 80.3% of the listed component irreversibilities, and therefore remains the dominant second-law loss.

4-6- Monte Carlo uncertainty propagation

A Monte Carlo uncertainty-propagation analysis was performed to complement the local one-at-a-time sensitivity analysis and to account for simultaneous variation of key uncertain model parameters. The analysis was conducted around the retained NASA7-constrained design point, which was independently reproduced by the revised optimization rerun; the decision variables were held fixed while uncertain component and boundary-condition parameters were sampled simultaneously. The Monte Carlo analysis therefore quantifies output uncertainty around the identified design point rather than performing a separate robust re-optimization for every realization.

For each realization, the temperature-dependent exhaust-mixture model described in Section 3 was used to calculate the available heat and hot-stream physical-exergy decrease at the sampled stack temperature. Turbine and pump work were recalculated using the sampled isentropic efficiencies, and the corresponding ORC mass flow rate was determined from the available HRVG heat duty. A total of 50,000 independent realizations were evaluated using a fixed random seed of 2026. Increasing the sample count from 20,000 to 50,000 changed the mean net-power estimate by less than 0.04%, indicating adequate statistical convergence for the reported quantities. The deterministic revised design gives a net power of 6119.49 kW and a net physical-exergy recovery ratio, ψ_{rec}, of 33.58%. The Monte Carlo population gives a mean net power of 6118.60 kW with a standard deviation of 194.78 kW. The corresponding 2.5th and 97.5th percentiles are 5747.68 and 6502.19 kW, respectively, giving a 95% uncertainty interval of approximately −6.08% to +6.25% relative to the deterministic value. The net physical-exergy recovery ratio, ψ_{rec}, has a mean of 33.582%, a standard deviation of 0.925 percentage points and a 95% interval of 31.825–35.370%.

Rank-correlation analysis confirms that turbine efficiency is the dominant uncertainty driver. The Spearman correlation coefficients of η_t, $T_{stack,min}$ and η_p with net power are +0.807, −0.562 and +0.046, respectively. For ψ_{rec}, the corresponding coefficients are +0.938, −0.321 and +0.054. Thus, uncertainty in turbine performance dominates both reported outputs, while the stack-temperature requirement has a secondary but non-negligible influence and pump-efficiency uncertainty is comparatively minor. The stochastic analysis therefore supports the qualitative conclusions of the previous sensitivity assessment while providing simultaneous uncertainty bounds that cannot be obtained from OAT perturbations alone.

Table 7 Input distributions adopted for the Monte Carlo uncertainty analysis.

Parameter	Distribution	Lower bound	Mode	Upper bound
η_t	Triangular	0.80	0.85	0.90
η_p	Triangular	0.70	0.75	0.80
$T_{stack,min}$ (°C)	Triangular	100	120	140

Table 8 Monte Carlo uncertainty-propagation results for the revised design (N=50,000)

Output	Deterministic	Mean	Standard deviation	2.5th percentile	97.5th percentile
$\dot{W}_{net}$	6119.49	6118.60	194.78	5747.68	6502.19
ψ_{rec} (%)	33.58	33.582	0.925	31.825	35.370

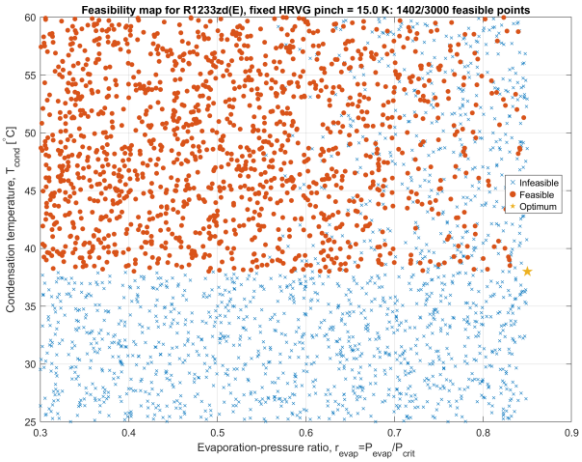


Fig. 1 Feasibility map from the original 3000-point three-variable design-space scan. The independent NASA7-based scan produced a closely similar feasible fraction (47.17% versus 46.73% in the original scan) and confirmed the same boundary-controlled design-space interpretation.

5- Results and analysis

5-1- Feasibility of the constrained design space

The original 3000-point feasibility scan classified 1402 points as feasible and 1598 as infeasible, corresponding to a feasible fraction of 46.73%; Fig. 1 retains this original scan because it documents the design-space screening used during development of the initial constrained search. As an independent cross-check after introduction of the temperature-dependent NASA7 exhaust model, a new 3000-point uniformly sampled feasibility scan was performed within the same variable bounds. The independent rerun classified 1415 points as feasible and 1585 as infeasible, corresponding to a feasible fraction of 47.17%. Because the independent implementation uses its own random-number sequence, the two scans are compared statistically rather than point by point. Their closely matched feasible fractions support the conclusion that the revised exhaust-property model does not materially alter the overall constrained character of the design space.

The rejected candidates in the NASA7-based rerun were again dominated by condenser-approach and critical-temperature-margin violations. The identified optimum remains located at the high r_{evap}, low- T_{cond} boundary of the feasible domain, consistent with the physical tendency of increasing evaporation pressure and decreasing condensation temperature to improve cycle work until active constraints are encountered.

5-2- Independent NASA7 differential-evolution rerun and convergence verification

After introduction of the fixed-composition, temperature-dependent NASA7 exhaust model, the three-variable constrained optimization was independently reconstructed and rerun using the DE settings specified in Section 3.2. The best feasible net power increased rapidly during the early generations and approached the final boundary solution well before completion of the 120-generation computational budget. By generation 80, the best feasible value had reached approximately 6119.35 kW; subsequent improvement was only about 0.13 kW, and the final value after 120 generations was 6119.480 kW. The best DE individual after 120 generations was r_{evap} =0.849957, T_{cond} =38.000009°C and ΔT_{sh} =4.582929 K, giving $\dot{W}_{net}$=6119.480 kW. A subsequent numerical refinement of the active boundary gave r_{evap}=0.850000, T_{cond}=38.000000°C , ΔT_{sh} =4.580064 K, with $\dot{W}_{net}$ =6119.489 kW and η_{th}=16.38775%. This independently reproduced solution is numerically indistinguishable from the retained manuscript design r_{evap}=0.849996, T_{cond} =38.000 °C, ΔT_{sh} =4.5797 K, for which the detailed state-point model gives 6119.491 kW. The independent rerun therefore confirms the robustness of the constraint-controlled boundary solution under the NASA7 source-property formulation.

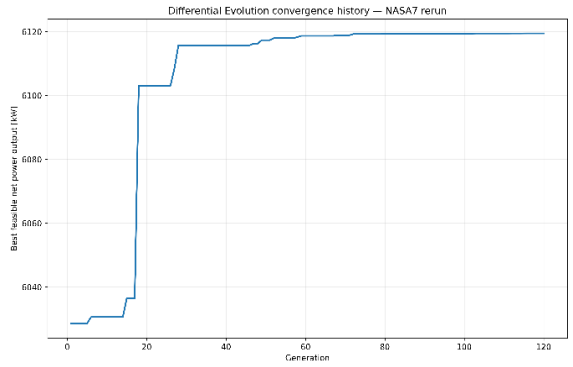


Fig. 2 Best-feasible net-power convergence history from the independent NASA7-based differential-evolution rerun (F=0.70, CR=0.9, population size = 50, and 120 generations). The convergence trajectory approaches 6119.480 kW and independently reproduces the same constraint-controlled boundary solution as the retained manuscript design.

5-3- NASA7-constrained design and performance

Table 9 summarizes the retained NASA7-constrained design used for the detailed thermodynamic, exergy, uncertainty, and economic calculations. The independent optimization rerun reproduced this point within numerical tolerance: the final DE individual gives 6119.480 kW and the active-boundary refinement gives 6119.489 kW, compared with 6119.491 kW for the retained detailed state-point evaluation. Because these differences are negligible relative to the reporting precision of the cycle model, the detailed design vector and state-point values are retained in Tables 9 and 10 for consistency with the subsequent analyses. The stack-temperature limit, condenser approach, and critical-temperature safety margin remain active, whereas the fixed HRVG pinch remains inactive with a large positive margin.

Table 9 Performance indicators at the retained NASA7-constrained R1233zd(E) design point independently reproduced by the optimization rerun.

Quantity	Value	Unit
Working fluid	R1233zd(E)	-
HRVG flow arrangement	Counter-flow	-
r_{evap}	0.849996	-
T_{cond}	38.000	°C
ΔT_{sh}	4.5797	K
Fixed HRVG pinch	15	K
P_{evap}	30.8012	bar
P_{cond}	2.0212	bar
$T_{turbine, in}$	161.4508	°C
$T_{turbine, out}$	63.2667	°C
$T_{hot, in}$	543	°C
$T_{hot, out}$	120	°C
$T_{stack, min}$	120	°C
Turbine power	6590.293	kW
Pump power	470.801	kW
Net power	6119.491	kW
Heat input in HRVG	37341.86	kW
Heat rejected in condenser	31222.373	kW
Thermal efficiency	16.3877	%
ORC mass flow rate	151.4176	kg s^{-1}
Cooling-water mass flow rate	1493.893	kg s^{-1}
Minimum HRVG temperature difference	80.1789	K
Minimum condenser temperature difference	8.0000	K
Turbine-outlet phase	Superheated	-

The relatively high cooling-water mass flow rate is a direct consequence of the assumed 5 K cooling-water temperature rise and the revised condenser duty of approximately 31.22 MW. The corresponding cooling-water requirement is approximately 1493.89 kg s^{-1}. This should not be interpreted as a numerical inconsistency; rather, it identifies the cooling system as an important plant-level design issue.

5-4- State points and T-s behavior

The state points in Table 10 show that the turbine inlet is only slightly superheated above the saturated-vapor state at the evaporation pressure. The turbine outlet remains superheated, so the dryness constraint is satisfied with margin. The independently reproduced NASA7-constrained solution retains essentially the same thermodynamic state structure as the detailed retained design. At the turbine inlet, the pressure is approximately 30.801 bar and the temperature is approximately 161.451 °C, placing the state close to the imposed critical-temperature safety limit. Following expansion, the turbine outlet remains superheated at approximately 63.267 °C, confirming that wet expansion does not constrain the optimum.

Fig. 3 shows the identified cycle design on a T-s diagram. The turbine-inlet temperature is approximately 161.45 °C, which is essentially equal to the imposed limit T_{crit} - 5 K because the critical temperature of R1233zd(E) is 166.45 °C.

5-5- HRVG temperature matching and exergy implication

Fig. 4 is the key diagnostic figure of the corrected counter-flow HRVG model. The cold end pairs the 120 °C stack gas with the pump-outlet liquid, while the hot end pairs the 543 °C exhaust inlet with the turbine-inlet vapor. The actual minimum temperature difference is 80.18 K, much larger than the fixed 15 K constraint.

Table 10 Thermodynamic state points at the retained NASA7-constrained R1233zd(E) design point.

State	Description	P (bar)	T (°C)	h (kJ/kg)	s (kJ kg^{-1} K^{-1})	q	Phase note
1	Condenser outlet	2.02116	38.000	245.905	1.15685	0.000	Saturated liquid
2	Pump outlet	30.80123	9.8211249.014		1.15934	—	Compressed liquid
3	Saturated vapor	30.8012	156.871483.916		1.76598	1.000	Saturated vapor
4	Turbine inlet	30.8012	161.451495.629		1.79308	—	Superheated
5	Turbine outlet	2.0415	763.2667452.105		1.81621	—	Superheated
6	Condenser inlet	2.0211	663.2185452.105		1.81682	—	Condenser inlet

The large temperature mismatch in Fig. 4 is a physical consequence of using a relatively low-critical-temperature fluid with a 543 °C exhaust source in a simple subcritical ORC. The cycle can cool the exhaust stream to the imposed stack temperature, but it cannot match the high exergy level of the hot stream efficiently because the

maximum allowable turbine-inlet temperature is limited by the fluid critical temperature.

5-6- Condenser behavior and cooling-water requirement

The condenser constraint is also active. The optimized condensation temperature is approximately 38 °C, while the cooling water exits at 30 °C. Therefore, the minimum condenser approach is 8 K. This explains why reducing T_{cond} in the OAT analysis is infeasible.

For the assumed cooling-water temperature increase of only 5 K, the revised condenser duty of approximately 31.22 MW requires about 1493.89 kg s^{-1} of cooling water. This remains a large industrial flow rate and should be considered a practical limitation of the selected boundary conditions. Detailed plant design should evaluate alternative cooling-water temperature rises, air-cooled condensers, or hybrid cooling options.

5-7- Quantitative exergy analysis

The quantitative exergy analysis in Table 11 provides the second-law basis for interpreting the retained NASA7-constrained boundary solution. The hot-gas physical-exergy decrease between 543 °C and 120 °C is approximately 18.22 MW, and the corresponding net physical-exergy recovery ratio is 33.58%. The HRVG remains the dominant exergy-destruction component, accounting for approximately 80.3% of the listed component irreversibilities. This confirms that the principal second-law penalty is associated with the large source–working-fluid temperature mismatch rather than with turbine wetness or an insufficient HRVG pinch.

Table 11 Quantitative exergy assessment at the retained NASA7-constrained R1233zd(E) design point.

Quantity	Value	Unit	Interpretation
Hot-gas physical-exergy decrease	18222.88	kW	Physical-exergy decrease over the imposed cooling interval
HRVG exergy destruction	9491.32	kW	Dominant irreversibility due to source–working-fluid temperature mismatch
Turbine exergy destruction	1044.22	kW	Loss associated with non-isentropic expansion
Pump exergy destruction	112.45	kW	Small contribution
Condenser exergy destruction	1168.95	kW	Includes finite-temperature rejection to cooling water
Listed component exergy destruction total	11816.94	kW	Sum of HRVG, turbine, pump and condenser destruction
Net physical-exergy recovery ratio, ψ_{rec}	33.58	%	$\frac{\dot{W}net}{\Delta \dot{E}^{ph}_{x,h}}$

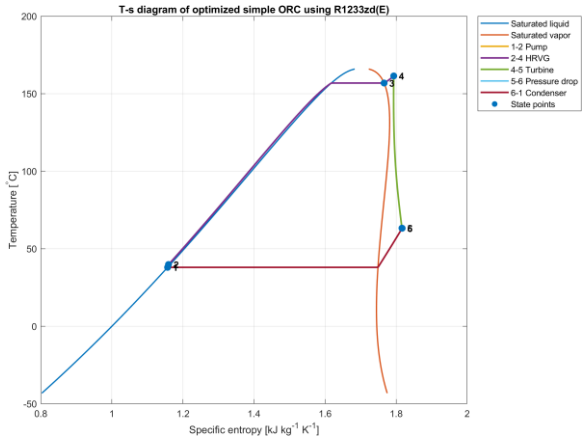


Fig. 3 T-s diagram of the identified R1233zd(E) ORC design. The turbine-inlet state is near the imposed critical-temperature safety margin, and the turbine outlet remains superheated.

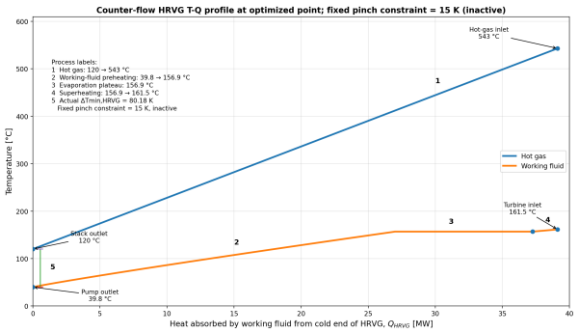


Fig. 4 Counter-flow HRVG T-Q diagram for the identified R1233zd(E) ORC design. The actual minimum HRVG temperature difference is much larger than the fixed 15 K pinch constraint, so the HRVG pinch is inactive.

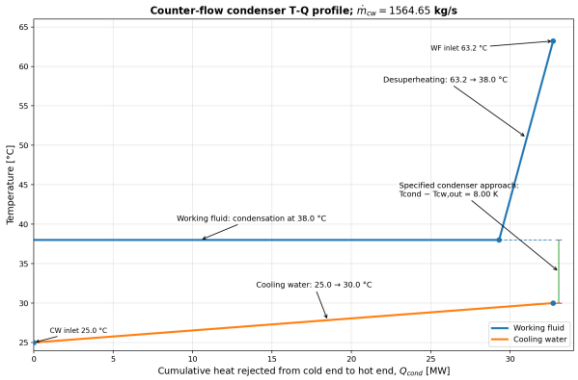


Fig. 5 Condenser T-Q diagram for the retained R1233zd(E) ORC design. The minimum cooling-water approach is active and equal to approximately 8 K

This exergy distribution confirms that the primary thermodynamic penalty is not wet expansion or insufficient HRVG pinch. Instead, it is the mismatch between the high-temperature exhaust profile and the limited allowable turbine-inlet temperature of R1233zd(E). Therefore, improving the system would require architecture or fluid changes rather than merely reducing the HRVG pinch. The residual between the hot-gas physical-exergy decrease, the revised net power and the listed component exergy destructions is approximately 286.45 kW, corresponding to about 1.57% of the hot-gas physical-exergy decrease. This residual is attributed to simplified auxiliary-stream exergy treatment, pressure-adjustment states and numerical rounding. Accordingly, Table 11 should be interpreted as a component-level exergy assessment rather than as a complete plant exergy balance.

5-8- Constraint margins and active design limits

The active-constraint interpretation is summarized directly by the constraint margins. Three constraints are active: stack temperature, condenser approach and critical-temperature safety margin. The HRVG pinch has a positive margin of 65.18 K and is inactive.

The numerical constraint margins confirm the boundary nature of the identified constrained design point : $T_{hot,out} - T_{stack,min} = 0.000$ K, $\Delta T_{min,cond} - \Delta T_{approach,min} = 4.734e\text{-}05$ K and $T_{crit-margin} - T_{turbine,in} = 5.882e\text{-}05$ K are active within numerical tolerance. In contrast, the turbine-outlet dryness margin is 0.120 and the HRVG pinch margin is 65.1789 K, confirming that wet expansion and HRVG pinch do not control the identified constrained design point. The corresponding revised net power at this identified boundary point is 6119.491 kW.

This constraint pattern is central to the interpretation of the identified constrained design. The identified constrained design is the best simple R1233zd(E) case under the defined constraints; it is not the best possible thermodynamic use of a 543 °C exhaust stream.

5-9- Morris-type constrained screening with the revised NASA7 model

The Morris-type constrained screening was rerun using the independently reconstructed NASA7-based cycle model with the same normalized perturbation size of 0.20 and feasibility rules described in Section 3.2. Elementary effects were retained only when both the base and perturbed points were feasible, resulting in 15 valid effects for r_{evap}, 22 for T_{cond}, and 19 for ΔT_{sh}.

The revised screening gives μ=1802.037, $\mu*$=1802.037, and σ=571.022 for r_{evap}; μ=−1965.497, $\mu*$=1965.497, and σ=98.058 for T_{cond}; and μ=55.913, $\mu*$=63.295, and σ=78.637 for ΔT_{sh}. Thus, condensation temperature and evaporation-pressure ratio remain the dominant variables, whereas superheating has a substantially smaller absolute elementary effect. The revised NASA7 rerun therefore preserves the sensitivity ranking obtained in the earlier design-stage screening without relying on a scaling transformation of the original indices.

The absolute mean elementary effect $\mu*$ is largest for condensation temperature, followed by evaporation-pressure ratio, while the influence of superheating is substantially smaller. The corresponding standard deviations quantify the spread of the feasible elementary effects.

5-10- Local OAT sensitivity with the revised NASA7 model

The local one-at-a-time (OAT) sensitivity analysis was rerun using the revised NASA7-based cycle model and the perturbations defined in Section 3.2. Decreasing r_{evap} from 0.849996 to 0.794996 is feasible and gives 6048.189 kW, corresponding to a net-power reduction of 71.290 kW (1.16497%). Increasing r_{evap} is clipped by the upper search bound or becomes infeasible.

Decreasing T_{cond} from 38.0 to 34.5 °C violates the condenser-approach constraint, whereas increasing T_{cond} to 41.5 °C is feasible and gives 5941.330 kW, corresponding to a reduction of 178.149 kW (2.91118%). Decreasing ΔT_{sh} from 4.5797 to 1.5797 K is feasible and gives 6065.597 kW, corresponding to a reduction of 53.882 kW (0.88050%), whereas increasing superheating to 7.5797 K violates the critical-temperature safety margin.

These rerun results confirm the boundary-controlled character of the identified design: every feasible perturbation away from the optimum reduces the objective, while the opposite performance-improving directions are blocked by the evaporation-pressure upper bound, condenser-approach constraint, or critical-temperature safety margin

Feasible perturbations reduce net power by approximately 71.3 kW for lower evaporation-pressure ratio, 178.1 kW for higher condensation temperature, and 53.9 kW for lower superheating; the opposite directions are clipped or infeasible because of active constraints.

5-11- Pressure-drop and heat-loss sensitivity

Pressure losses in heat exchangers and connecting lines reduce the pressure ratio available to the expander and are unavoidable in practical ORC systems. Because the present cycle-level model does not include geometry-resolved HRVG, condenser and piping models, a parametric pressure-loss sensitivity was performed rather than assigning geometry-derived pressure losses that cannot be supported by the available design information. The original 1% low-side pressure adjustment was retained in the revised reference case, while additional HRVG and low-side pressure-drop ratios up to 5% were examined.

At the retained NASA7-constrained design point, which was independently reproduced by the optimization rerun, the turbine-inlet pressure is approximately 30.801 bar and the low-side turbine pressure is approximately 2.04 bar.

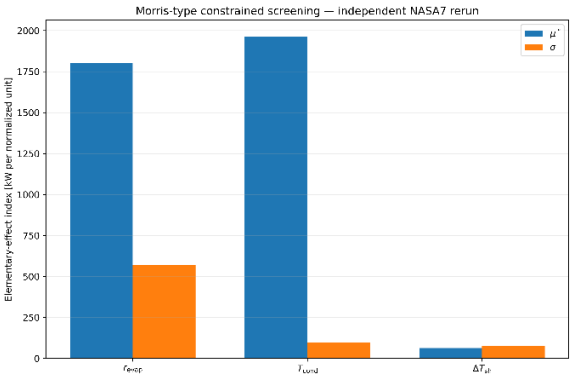


Fig. 6 Morris-type constrained screening from the independent NASA7-based rerun.

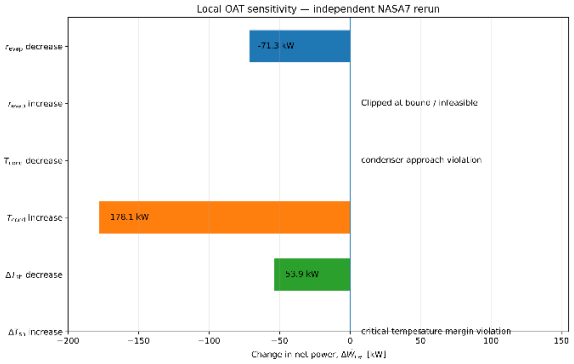


Fig. 7 Local OAT sensitivity from the independent NASA7-based rerun around the retained constrained design.

Table 12 Fixed-design sensitivity of the revised R1233zd(E) cycle to working-fluid pressure losses.

Case	HRVG pressure drop	Low-side pressure drop	Net power (kW)	Change from reference
Reference	0%	1%	6119.49	0
Mild	1%	1%	6113.19	−0.10%
Moderate	3%	3%	6047.46	−1.18%
Conservative screening	5%	5%	5978.65	−2.30%

Introducing a 1% HRVG pressure loss while retaining the reference 1% low-side pressure adjustment reduces the net power from 6119.49 to approximately 6113.19 kW. When both the HRVG and low-side pressure-loss ratios are increased to 3%, the calculated net power decreases to approximately 6047.46 kW, corresponding to a reduction of 1.18%. For the deliberately conservative 5% screening case, the net power decreases to approximately 5978.65 kW, or about 2.30% below the revised reference value.

A separate external HRVG heat-loss sensitivity gives net powers of approximately 6058.30 and 5997.10 kW for heat-loss fractions of 1% and 2%, respectively. Thus, both pressure losses and external heat leakage reduce the predicted cycle output, but the investigated screening ranges do not alter the main physical interpretation of the optimized design. The stack-temperature, condenser-approach and critical-temperature boundaries remain the dominant limitations, whereas the nominal HRVG pinch remains inactive.

The present results should be interpreted as cycle-level robustness estimates rather than equipment-level pressure-drop predictions. Detailed HRVG, condenser and piping geometries would be required before appropriate single- and two-phase pressure-drop correlations could be selected and applied and site-specific heat losses could be determined.

5-12- Same-source comparison with a higher-critical-temperature working fluid

To examine whether the low critical temperature of R1233zd(E) is central to the high-temperature mismatch identified above, the revised R1233zd(E) result was compared with an independently optimized higher-critical-temperature ORC reported for the same exhaust source. Chaczykowski [18] investigated ORC recovery from the same SGT-600 exhaust conditions adopted here, namely an exhaust temperature of 543 °C and a mass flow rate of 80.4 kg s^{-1}, and screened a range of higher-temperature organic working fluids. Among the promising subcritical candidates, toluene is particularly informative for the present comparison because its critical temperature is 318.60 °C, approximately 152 K higher than that of R1233zd(E).

For the revised R1233zd(E) baseline, the critical-temperature safety constraint limits the turbine-inlet temperature to 161.45 °C, leaving a hot-end source-to-working-fluid temperature difference of 381.55 K. The optimized subcritical toluene case reported for the same exhaust source operates at a turbine-inlet temperature of 281.1 °C, reducing the corresponding hot-end temperature difference to 261.9 K. This represents a reduction of approximately 31.4% in the source-to-turbine-inlet temperature mismatch. The same-source toluene study reports a plant net power of 9.86 MW and a thermal efficiency of 23.4%, whereas the revised simple R1233zd(E) baseline gives 6.119 MW and 16.388%, respectively.

These numerical differences should not be interpreted as a controlled fluid-only performance ratio because the two studies employ different heat-transfer and heat-rejection arrangements. The literature case uses an intermediate heat-transfer-fluid loop, a 30 °C condensing temperature and a forced-draft air condenser, whereas the present model uses a direct counter-flow HRVG and a cooling-water condenser at 38 °C. Nevertheless, the comparison is particularly useful because the exhaust inlet temperature and mass flow rate are identical. It independently supports the physical interpretation that the relatively low critical temperature of R1233zd(E) limits the attainable turbine-inlet temperature and aggravates source–working-fluid temperature mismatch when a simple subcritical cycle is coupled to this high-temperature source.

The same trend is consistent with a recent high-temperature ORC study at an exhaust temperature of 515.14 °C, in which toluene provided the highest simple-ORC performance among the investigated higher-temperature fluids, reaching a reported thermal efficiency of 24.33%; the same study also demonstrated the additional heat-recovery potential of a series ORC configuration [26].

Table 13 Same-source comparison of the revised R1233zd(E) baseline with the optimized subcritical toluene ORC reported by Chaczykowski [18].

Parameter	Present R1233zd(E)	Published toluene case
Exhaust inlet temperature (°C)	543	543
Exhaust mass flow rate (kg s^{-1})	80.4	80.4
Working-fluid critical temperature (°C)	166.45	318.60
Turbine-inlet temperature (°C)	161.45	281.1
Hot-source/TIT temperature difference (K)	381.55	261.90
Condensation temperature (°C)	38	30
Heat supplied to cycle / HTF (MW)	37.342	41.50
Net/plant power (MW)	6.119	9.86
Thermal efficiency (%)	16.388	23.4
Heat-source coupling	Direct counter-flow HRVG	Intermediate HTF loop
Heat rejection	Cooling water	Forced-draft air cooler

Table 14 Sensitivity of the screening LCOE to installed ORC cost.

Case	Specific CAPEX (M€/MW)	Total CAPEX (M€)	O&M (% CAPEX/y)	LCOE (€/MWh)
Low-cost	2.20	13.463	1.00	30.76
Baseline	2.75	16.829	1.25	39.31
High-cost	3.30	20.194	1.50	48.20

Table 15 Sensitivity of the baseline economic case to the credited electricity value.

Electricity value (€/kWh)	Gross electricity value (M€/y)	Net annual benefit after O&M (M€/y)	Simple payback (y)	20-y NPV (M€)
0.06	2.937	2.727	6.17	9.95
0.08	3.916	3.706	4.54	19.56
0.10	4.896	4.685	3.59	29.17
0.12	5.875	5.664	2.97	38.78

5-13- Preliminary economic screening

At the revised cycle net power of 6.11949 MW and 8000 annual operating hours, the expected annual electricity generation is 48.956 GWh. Using the baseline specific installed cost of 2.75 M€ MW^{-1} gives an estimated installed capital requirement of 16.829 M€, while the corresponding annual O&M cost is approximately 0.210 M€ yr^{-1}. For a 20-year project life and an 8% discount rate, the resulting screening LCOE is 39.31 € MWh^{-1}.

The uncertainty in installed cost remains important. Using the literature-based low and high cost cases of 2.20 and 3.30 M€ MW^{-1} gives total installed costs of 13.463 and 20.194 M€, respectively. When the associated O&M fractions of 1.0% and 1.5% are applied, the corresponding LCOE range is 30.76–48.20 € MWh^{-1}. Thus, the economic conclusion is not based on a single assumed capital cost.

At the baseline investment case, an avoided electricity value of 0.10 € kWh^{-1} corresponds to a gross annual electricity value of approximately 4.896 M€ yr^{-1}. After the assumed O&M expenditure, the annual net benefit is approximately 4.685 M€ yr^{-1}, giving a simple payback period of 3.59 years and a 20-year NPV of approximately 29.17 M€ at the adopted 8% discount rate. Because electricity value is location- and contract-dependent, Table 15 reports the corresponding sensitivity rather than treating 0.10 € kWh^{-1} as a universal tariff.

These results indicate that the thermodynamically constrained R1233zd(E) baseline can still be economically interesting when the recovered electricity displaces sufficiently valuable purchased power. Nevertheless, the present economic assessment remains preliminary. In particular, the thermodynamic net power includes the ORC working-fluid pump but does not resolve site-specific external cooling-water pumping, heat-recovery-system pressure losses, electrical balance-of-plant loads, detailed equipment sizing or local construction costs. A detailed project assessment could therefore produce a higher plant-level LCOE than the cycle-level screening value reported here.

6- Interpretation and engineering discussion

The results indicate that R1233zd(E) can generate meaningful power from the specified exhaust stream, but the simple subcritical layout cannot thermally match the high source temperature efficiently. The limiting factor is not a small evaporator pinch. Instead, the fluid reaches its maximum allowable turbine-inlet temperature while the exhaust stream still has a much higher temperature level, a limitation that is consistent with the role of critical properties in ORC working-fluid selection [3].

The independent NASA7-based optimization rerun reproduces the same constraint-controlled boundary solution within numerical tolerance. The 120-generation DE rerun converges to 6119.480 kW at r_{evap}=0.849957, T_{cond}=38.000009°C, and ΔT_{sh}=4.582929, while active-boundary refinement gives 6119.489 kW. Both results are numerically indistinguishable from the retained detailed design value of 6119.491 kW. This independent reproduction confirms that the principal

physical interpretation is robust to the temperature-dependent combustion-product property treatment: the simple R1233zd(E) cycle remains limited primarily by the low allowable working-fluid temperature relative to the 543 °C exhaust source rather than by the imposed HRVG pinch. It should not be described as the best possible use of a 543 °C source, nor should it be used to argue that R1233zd(E) is the best working fluid for such a source. The same-source comparison in Section 5.12 supports this interpretation: the independently optimized subcritical toluene case reaches a substantially higher turbine-inlet temperature and reports higher power and thermal efficiency for the same 543 °C, 80.4 kg s^{-1} exhaust source. Because the two models use different heat-transfer and cooling arrangements, this benchmark is not interpreted as a controlled working-fluid ranking; rather, it provides independent evidence that a higher allowable working-fluid temperature can improve utilization of this high-temperature source. Fully controlled comparisons involving recuperated, cascade, transcritical, or multi-pressure architectures remain appropriate extensions of the present work.

A conventional water/steam Rankine cycle is also an important reference alternative for the present 543 °C exhaust source. Its principal thermodynamic advantage relative to the investigated R1233zd(E) cycle is the possibility of operating at a much higher turbine-inlet temperature, thereby potentially reducing the extreme source–working-fluid temperature-level mismatch observed in Fig. 4. Nevertheless, steam is not automatically the optimum choice solely because the exhaust inlet temperature is high. Reviews of Rankine-cycle technologies show that cycle suitability depends strongly on heat-source characteristics, temperature matching, and cycle architecture [4, 7]. A recent study for gas-turbine exhaust at approximately 509 °C also found that a combined steam–organic arrangement can outperform the corresponding standalone configurations when thermodynamic and economic criteria are considered together [27]. Therefore, the present R1233zd(E) results should be interpreted as a deliberately constrained baseline that exposes the limitations of a simple low-critical-temperature ORC, rather than as a demonstration that ORC is intrinsically preferable to steam for this heat source.

The condenser result is also important for practical design. The revised cooling-water flow rate of approximately 1493.89 kg s^{-1} remains large and would strongly affect condenser size, auxiliary pumping, water availability and plant integration. A future design-oriented study should include cooling-system optimization rather than fixing the water temperature rise at 5 K [28].

The verification and benchmarking strategy also defines the appropriate confidence level of the results. The retained R245fa case supports the internal consistency of the ORC calculation framework [25], while the R1233zd(E)-specific literature benchmark supports the choice of R1233zd(E) as an ORC-capable low-GWP fluid [9–13, 17]. However, neither comparison directly validates a 543 °C, 6.12 MW high-temperature exhaust application. Therefore, the optimized state points should be regarded as numerically cross-checked and literature-benchmarked cycle-level predictions rather than as experimentally validated equipment-level design data. Before industrial implementation, they should be coupled with component-level expander modeling, detailed heat-exchanger sizing, pressure-drop correlations, cooling-system design and off-design simulations [28].

7- Limitations and future work

• The heat source is represented as a fixed-composition SGT-600-derived combustion-product mixture with temperature-dependent ideal-gas properties. This treatment is more realistic than the original constant-c_p, air-like representation, but it still neglects variations in exhaust composition, pressure, humidity and gas-turbine load. Future plant-specific studies should therefore use measured exhaust composition and operating data when available.

• Working-fluid pressure losses and external HRVG heat loss have been quantified through a dedicated fixed-design sensitivity analysis. Increasing both the HRVG and low-side pressure-loss ratios to 5% reduces the predicted net power by approximately 2.30%, while a 2% external HRVG heat loss produces an approximately 2% power penalty. These losses are imposed parametrically rather than calculated from equipment geometry; therefore, detailed HRVG, condenser and piping design with appropriate single- and two-phase pressure-drop correlations remains necessary before equipment-level design conclusions can be drawn.

• The turbine and pump isentropic efficiencies are fixed in the present cycle-level model. Future work should couple the thermodynamic model to geometry-dependent turbomachinery and pump performance maps, including off-design efficiency variation [3, 28].

• The added economic assessment is intentionally limited to screening-level feasibility. Installed cost and O&M are represented by literature-based ranges rather than component-by-component vendor quotations, and taxes, financing structure, price escalation, replacement costs and detailed balance-of-plant auxiliaries are excluded. Consequently, the reported LCOE, NPV and payback period should not be interpreted as bankable project estimates. Detailed heat-exchanger sizing, turbomachinery selection, cooling-system design and site-specific quotations are required for a definitive techno-economic assessment.

• The verification strategy combines first-law balance closure, an independent NASA7-based numerical rerun of the constrained optimization and sensitivity workflow, a direct numerical reconstruction of an independently published R1233zd(E) ORC case [24], an R245fa experimental model-consistency check [25], and a high-temperature same-fluid quantitative benchmark against Mariani et al. [29]. Together, these checks strengthen confidence in the cycle-level thermodynamic calculations and in the robustness of the identified boundary solution; however, none constitutes direct experimental validation of the complete present 543 °C MW-scale application.

• A same-source literature comparison with higher-critical-temperature toluene has been included to test the physical interpretation of the R1233zd(E) temperature mismatch. The comparison supports the benefit of a higher attainable turbine-inlet temperature, but differences in the heat-transfer loop, condenser conditions and auxiliary loads prevent it from being interpreted as a controlled fluid-only ranking. Future work should therefore perform a common-boundary re-optimization of multiple working fluids and advanced recuperated, cascade, transcritical or multi-pressure architectures.

• Future experimental validation should target an R1233zd(E) ORC operating near the identified constrained design point, with r_{evap} ≈0.85, T_{cond} ≈ 38°C, a turbine-inlet temperature near 161.45 °C and a high-temperature exhaust source representative of the 543 °C boundary condition. The test facility should measure pressures and temperatures at the principal ORC state points, working-fluid and heat-source mass flow rates, turbine and pump power, HRVG and condenser pressure losses, and multi-point HRVG temperatures. Validation should compare net power, heat duties, thermal efficiency, the net physical-exergy recovery ratio and the minimum HRVG temperature difference with model predictions. At least two feasible off-design conditions, involving a lower evaporation-pressure ratio and a higher condensation temperature, should also be tested to assess whether the model reproduces measured performance trends rather than only one nominal operating point.

8- Conclusion

1. A three-variable constrained optimization of a simple subcritical R1233zd(E) ORC was performed using a counter-flow HRVG with a fixed 15 K minimum pinch constraint.
2. An independent rerun of the constrained optimization using the fixed-composition, temperature-dependent NASA7 combustion-product exhaust model reproduces the same boundary solution within numerical tolerance. The 120-generation DE rerun converges to 6119.480 kW at an evaporation-pressure ratio of 0.849957, a condensation temperature of 38.000009 °C, and a superheating degree of 4.582929 K. Active-boundary refinement gives 6119.489 kW at an evaporation-pressure ratio of 0.850000, a condensation temperature of 38.000000 °C, and a superheating degree of 4.580064 K, independently reproducing the retained detailed design value of 6119.491 kW and 16.388% thermal efficiency.
3. At the retained NASA7-constrained design point, the 120 °C minimum stack-temperature limit, the condenser-approach constraint, and the R1233zd(E) critical-temperature safety margin are active.
4. The fixed 15 K HRVG pinch constraint remains inactive at this design point. The actual minimum HRVG temperature difference is approximately 80.18 K, corresponding to a margin of about 65.18 K above the imposed minimum.
5. A same-source benchmark against an independently optimized subcritical toluene ORC supports the temperature-mismatch interpretation. For identical exhaust inlet conditions of 543 °C and 80.4 kg s^{-1}, the published toluene case operates at a turbine-inlet temperature of 281.1 °C compared with 161.45 °C for R1233zd(E), reducing the hot-end source-to-working-fluid temperature difference from 381.55 to 261.9 K. The literature case reports 9.86 MW plant power and 23.4% thermal efficiency versus 6.119 MW and 16.388% for the present R1233zd(E) baseline; these differences are treated as a same-source benchmark rather than as a controlled fluid-only comparison because the heat-transfer and condenser arrangements differ.
6. The turbine outlet remains superheated at the identified design point, so the turbine-outlet dryness constraint is satisfied with margin.
7. The temperature-dependent exhaust model gives a hot-gas physical-exergy decrease of approximately 18.22 MW and a net physical-exergy recovery ratio of 33.58%. The HRVG remains the dominant component-level source of exergy destruction, accounting for approximately 80.3% of the listed component irreversibilities. The reported recovery ratio is deliberately distinguished from a complete plant exergetic efficiency because it is referenced to the physical-exergy decrease of the exhaust over the imposed cooling interval.
8. Morris-type constrained screening rerun with the revised NASA7 model confirms that condensation temperature and evaporation-pressure ratio dominate the constrained response. The corresponding μ^* values are 1965.497 for condensation temperature, 1802.037 for evaporation-pressure ratio, and 63.295 for superheating. The associated σ values are 98.058, 571.022, and 78.637, respectively. Thus, superheating has a substantially smaller absolute effect than the two dominant design variables.
9. Monte Carlo propagation with 50,000 simultaneous realizations gives a 95% net-power interval of 5.748–6.502 MW and a corresponding net physical-exergy recovery-ratio interval of 31.825–35.370%. Turbine isentropic efficiency is the dominant uncertainty driver, followed by the minimum stack-temperature requirement.
10. The NASA7-based local OAT rerun confirms the boundary-controlled character of the final design. Reducing the evaporation-pressure ratio to 0.794996 gives approximately 6048.189 kW, corresponding to a reduction of 71.290 kW (1.16497%); increasing the condensation temperature to 41.5 °C gives approximately 5941.330 kW, corresponding to a reduction of 178.149 kW (2.91118%); and reducing the superheating degree to 1.5797 K gives approximately 6065.597 kW, corresponding to a reduction of 53.882 kW (0.88050%). Perturbations in the opposite performance-improving directions are blocked by the evaporation-pressure upper bound, condenser-approach constraint, or critical-temperature safety margin.
11. A fixed-design pressure-loss sensitivity shows that a conservative case with 5% HRVG and 5% low-side pressure losses reduces the revised net power from 6.119 MW to approximately 5.979 MW (−2.30%). A separate 2% external HRVG heat-loss case reduces the predicted net power to approximately 5.997 MW. These penalties are moderate and do not change the identification of the dominant active constraints.
12. The present result should be interpreted as an identified constrained simple R1233zd(E) design under the specified assumptions, not as the best possible use of a 543 °C exhaust stream or as evidence that R1233zd(E) is preferable to water/steam or other candidate working fluids. The large source–working-fluid temperature mismatch motivates comparison with steam Rankine cycles, higher-critical-temperature fluids and advanced or combined cycle architectures.
13. A preliminary economic screening gives an annual electricity production of approximately 48.96 GWh for 8000 operating hours. Using a literature-based installed-cost range of 2.2–3.3 M€ MW^{-1} gives an estimated LCOE range of 30.8–48.2 € MWh^{-1}, with a baseline value of 39.3 € MWh^{-1}. At an illustrative credited electricity value of 0.10 € kWh^{-1}, the baseline case gives a simple payback period of approximately 3.6 years. These values represent screening-level economics and exclude detailed plant auxiliaries and site-specific equipment quotations.
14. The model has been strengthened through first-law balance checks, an independent NASA7-based numerical rerun of the constrained optimization and sensitivity analyses, a direct numerical R1233zd(E) literature reconstruction [24], an independent R245fa model-consistency benchmark [25], and a high-temperature same-fluid quantitative comparison with Mariani et al. [29]. Nevertheless, direct experimental validation of the complete present high-temperature MW-scale application remains unavailable. Future validation should reproduce the nominal pressure and temperature state of the identified cycle and at least two feasible off-design conditions while measuring the principal ORC state points, flow rates, component powers, pressure losses, and HRVG temperature profile.

Nomenclature

List of symbols and abbreviations

Symbol/abbreviation	Definition and dimensions
c_p	Specific heat capacity at constant pressure (kJ kg^{-1} K^{-1})
e	Specific physical exergy (kJ kg^{-1})
h	Specific enthalpy (kJ kg^{-1})
$\dot{m}$	Mass flow rate (kg s^{-1})
P	Pressure (Pa or bar, as stated)
q	Vapor quality or dryness indicator (–)
$\dot{Q}$	Heat-transfer rate (kW)
r_{evap}	Evaporation-pressure ratio relative to critical pressure (–)
s	Specific entropy (kJ kg^{-1} K^{-1})
T	Temperature (K or °C, as stated)
T_0	Environmental reference temperature (K)
T_{cond}	Condensation temperature (°C)
T_{crit}	Critical temperature (K)
$\dot{W}$	Power (kW)
ΔT_{app}	Condenser approach temperature difference (K)
ΔT_{pinch}	HRVG pinch-point temperature difference (K)
ΔT_{sh}	Superheating degree (K)
η_p	Pump isentropic efficiency (–)
η_t	Turbine isentropic efficiency (–)
η_{th}	Thermal efficiency (–)
ψ_{rec}	Net physical-exergy recovery ratio (–)

Artificial Intelligence Statement

The authors declare that no generative artificial intelligence tools were used in the preparation of this manuscript.

Acknowledgements

The authors have no acknowledgements to declare.

Funding

This research received no specific grant from any funding agency in the public, commercial, or not-for-profit sectors.

CRediT Authorship Contribution

Negin Sadat Hoseini Navid: *Conceptualization, Methodology, Software, Validation, Formal analysis, Investigation, Data curation, Visualization, Writing—original draft, Writing—review and editing.* ***Reza Taghavi Zenouz:*** *Conceptualization, Methodology, Validation, Supervision, Project administration, Writing—review and editing.*

Conflict of Interest

The authors declare that they have no known competing financial interests or personal relationships that could have influenced the work reported in this paper.

References

[1] S. Quoilin, M. Van Den Broek, S. Declaye, P. Dewallef, and V. Lemort, "Techno-economic survey of Organic Rankine Cycle (ORC) systems," Renewable and Sustainable Energy Reviews, vol. 22, pp. 168–186, 2013. doi: 10.1016/j.rser.2013.01.028.

[2] B. F. Tchanche, G. Lambrinos, A. Frangoudakis, and G. Papadakis, "Low-grade heat conversion into power using organic Rankine cycles: A review of various applications," Renewable and Sustainable Energy Reviews, vol. 15, no. 8, pp. 3963–3979, 2011. doi: 10.1016/j.rser.2011.07.024.

[3] J. Bao and L. Zhao, "A review of working fluid and expander selections for organic Rankine cycle," Renewable and Sustainable Energy Reviews, vol. 24, pp. 325–342, 2013. doi: 10.1016/j.rser.2013.03.040.

[4] E. Macchi and M. Astolfi, Eds., Organic Rankine Cycle (ORC) Power Systems: Technologies and Applications. Woodhead Publishing, 2016.

[5] A. Toffolo, A. Lazzaretto, G. Manente, and M. Paci, "A multi-criteria approach for the optimal selection of working fluid and design parameters in Organic Rankine Cycle systems," Applied Energy, vol. 121, pp. 219–232, 2014. doi: 10.1016/j.apenergy.2014.01.089.

[6] J. C. Jiménez-García, A. Ruiz, A. Pacheco-Reyes, and W. Rivera, "A Comprehensive Review of Organic Rankine Cycles," Processes, vol. 11, no. 7, 1982, 2023. doi: 10.3390/pr11071982.

[7] P. Colonna, E. Casati, C. Trapp, T. Mathijssen, J. Larjola, T. Turunen-Saaresti, and A. Uusitalo, "Organic Rankine Cycle power systems: From the concept to current technology, applications, and an outlook to the future," Journal of Engineering for Gas Turbines and Power, vol. 137, no. 10, 100801, 2015. doi: 10.1115/1.4029884.

[8] M. Lecompte, H. Huisseune, M. van den Broek, B. Vanslambrouck, and M. De Paepe, "Review of organic Rankine cycle (ORC) architectures for waste heat recovery," Renewable and Sustainable Energy Reviews, vol. 47, pp. 448–461, 2015. doi: 10.1016/j.rser.2015.03.089.

[9] S. Eyerer, C. Wieland, A. Vandersickel, and H. Spliethoff, "Experimental study of an ORC (Organic Rankine Cycle) and analysis of R1233zd-E as a drop-in replacement for R245fa for low temperature heat utilization," Energy, vol. 103, pp. 660–671, 2016. doi: 10.1016/j.energy.2016.03.034.

[10] J. Yang, Z. Sun, B. Yu, and J. Chen, "Experimental comparison and optimization guidance of R1233zd(E) as a drop-in replacement to R245fa for organic Rankine cycle application," Applied Thermal Engineering, vol. 141, pp. 10–19, 2018. doi: 10.1016/j.applthermaleng.2018.05.105.

[11] S. Eyerer, F. Dawo, J. Kaindl, C. Wieland, and H. Spliethoff, "Experimental investigation of modern ORC working fluids R1224yd(Z) and R1233zd(E) as replacements for R245fa," Applied Energy, vol. 240, pp. 946–963, 2019. doi: 10.1016/j.apenergy.2019.02.086.

[12] F. Dawo, J. Fleischmann, F. Kaufmann, C. Schifflechner, S. Eyerer, C. Wieland, and H. Spliethoff, "R1224yd(Z), R1233zd(E) and R1336mzz(Z) as replacements for R245fa: Experimental performance, interaction with lubricants and environmental impact," Applied Energy, vol. 288, 116661, 2021. doi: 10.1016/j.apenergy.2021.116661.

[13] M.-H. Yang, M.-C. Liu, and R.-H. Yeh, "Investigation of low-GWP working fluids as substitutes for R245fa in organic Rankine cycle application," Heliyon, vol. 10, no. 14, e34219, 2024. doi: 10.1016/j.heliyon.2024.e34219.

[14] M. Lampe, M. Stavrou, H. M. Bücker, J. Gross, and A. Bardow, "Simultaneous optimization of working fluid and process for Organic Rankine Cycles using PC-SAFT," Industrial & Engineering Chemistry Research, vol. 53, no. 21, pp. 8821–8830, 2014. doi: 10.1021/ie5006542.

[15] X. Zhang, X. Wang, P. Yuan, Z. Ling, X. Bian, J. Wang, H. Tian, and G. Shu, "Experimental study on the

comparative performance of R1233zd(E) and R123 for organic Rankine cycle for engine waste heat recovery," International Journal of Green Energy, vol. 21, no. 14, pp. 3305–3312, 2024. doi: 10.1080/15435075.2024.2376734.

[16] X. Li, Y. Chen, Y. Zhang, and Y. Liu, "Thermoeconomic modelling and multi-objective optimisation of ORC systems for low-temperature waste heat recovery," Applied Thermal Engineering, vol. 279, Part B, 127603, 2025. doi: 10.1016/j.applthermaleng.2025.127603.

[17] J. Yang, Z. Ye, B. Yu, H. Ouyang, and J. Chen, "Simultaneous experimental comparison of low-GWP refrigerants as drop-in replacements to R245fa for organic Rankine cycle application: R1234ze(Z), R1233zd(E), and R1336mzz(E)," Energy, vol. 173, pp. 721–731, 2019. doi: 10.1016/j.energy.2019.02.054.

[18] M. Chaczykowski, "Organic Rankine Cycle for Residual Heat to Power Conversion in Natural Gas Compressor Station. Part II: Plant Simulation and Optimisation Study," Archives of Mining Sciences, vol. 61, no. 2, pp. 259–274, 2016. doi: 10.1515/amsc-2016-0019.

[19] B. J. McBride, M. J. Zehe, and S. Gordon, NASA Glenn Coefficients for Calculating Thermodynamic Properties of Individual Species, NASA/TP-2002-211556, NASA Glenn Research Center, Cleveland, OH, USA, 2002.

[20] I. H. Bell, J. Wronski, S. Quoilin, and V. Lemort, "Pure and pseudo-pure fluid thermophysical property evaluation and the open-source thermophysical property library CoolProp," Industrial & Engineering Chemistry Research, vol. 53, no. 6, pp. 2498–2508, 2014. doi: 10.1021/ie4033999.

[21] R. Storn and K. Price, "Differential Evolution - A Simple and Efficient Heuristic for Global Optimization over Continuous Spaces," Journal of Global Optimization, vol. 11, no. 4, pp. 341–359, 1997. doi: 10.1023/A:1008202821328.

[22] M. D. Morris, "Factorial Sampling Plans for Preliminary Computational Experiments," Technometrics, vol. 33, no. 2, pp. 161–174, 1991. doi: 10.1080/00401706.1991.10484804.

[23] European Commission, "Waste Heat Recovery for Power Valorisation with Organic Rankine Cycle Technology in Energy Intensive Industries (TASIO)," CORDIS, Project 637189, 2020, accessed Sep. 20, 2026.

[24] K. Braimakis and S. Karellas, "Thermodynamic investigation of integrated organic Rankine cycle-ejector vapor compression cooling cycle waste heat recovery configurations for cooling, heating and power production," Energy, vol. 304, 132020, 2024. doi: 10.1016/j.energy.2024.132020.

[25] L. Li, Y. T. Ge, and S. A. Tassou, "Experimental Study on a Small-scale R245fa Organic Rankine Cycle System for Low-grade Thermal Energy Recovery," Energy Procedia, vol. 105, pp. 1827–1832, 2017. doi: 10.1016/j.egypro.2017.03.531.

[26] T. Klamrassamee, T. Kittijungjit, Y. Sukjai, and Y. Laoonual, "Thermodynamic, economic, and carbon emission evaluation of various Organic Rankine cycle configurations for maximizing waste heat recovery potential," Energy Conversion and Management: X, vol. 26, 100943, 2025. doi: 10.1016/j.ecmx.2025.100943.

[27] T. Kittijungjit, T. Klamrassamee, Y. Laoonual, and Y. Sukjai, "Comprehensive study on waste heat recovery from gas turbine exhaust using combined steam Rankine and organic Rankine cycles," Energy Conversion and Management: X, vol. 25, 100825, 2025. doi: 10.1016/j.ecmx.2024.100825.

[28] K. Rahbar, S. Mahmoud, R. K. Al-Dadah, N. Moazami, and S. A. Mirhadizadeh, "Review of organic Rankine cycle for small-scale applications," Energy Conversion and Management, vol. 134, pp. 135–155, 2017. doi: 10.1016/j.enconman.2016.12.023.

[29] A. Mariani, B. Morrone, D. Laiso, M. V. Prati, and A. Unich, "Waste Heat Recovery in a Compression Ignition Engine for Marine Application Using a Rankine Cycle Operating with an Innovative Organic Working Fluid," Energies, vol. 15, no. 21, 7912, 2022, doi: 10.3390/en15217912.